# Exploring Data Efficiency in Zero-Shot Learning with Diffusion Models

Zihan Ye<sup>1,2,4</sup>, Shreyank N. Gowda<sup>3</sup>, Xiaobo Jin<sup>1\*</sup>, Xiaowei Huang<sup>4</sup>, Haotian Xu<sup>1</sup>, Yaochu Jin<sup>2</sup>, Kaizhu Huang<sup>5</sup>

- <sup>1\*</sup>School of Advanced Technology, Xi'an Jiaotong-Liverpool University, 111 Ren'ai Road, Suzhou, 215123, Jiangsu, China.
  - <sup>2</sup>School of Engineering, Westlake University, No.600 Dunyu Road, Hangzhou, 310030, Zhejiang, China.
- <sup>3</sup>Department of Engineering Sciences, University of Oxford, Old Road Campus Research Building, Oxford, OX12JD, UK.
  - <sup>4</sup>Department of Computer Science, University of Liverpool, Ashton Street, Liverpool, L693BX, UK.
- <sup>5</sup>Data Science Research Center, Duke Kunshan University, No. 8 Duke Avenue, Suzhou, 215316, Jiangsu, China.

\*Corresponding author(s). E-mail(s): Xiaobo.Jin@xjtlu.edu.cn; Contributing authors: zihhye@outlook.com; kini5gowda@gmail.com; xiaowei.huang@liverpool.ac.uk; haotian37@qq.com; jinyaochu@westlake.edu.cn; kaizhu.huang@dukekunshan.edu.cn;

#### Abstract

Zero-Shot Learning (ZSL) aims to enable classifiers to identify unseen classes by enhancing data efficiency at the class level. This is achieved by generating image features from pre-defined semantics of unseen classes. However, most current approaches heavily depend on the number of samples from seen classes, i.e. they do not consider instance-level effectiveness. In this paper, we demonstrate that limited seen examples generally result in deteriorated performance of generative models. To overcome these challenges, we propose ZeroDiff, a Diffusion-based Generative ZSL model. This unified framework incorporates diffusion models to improve data efficiency at both the class and instance levels. Specifically, for instance-level effectiveness, ZeroDiff utilizes a forward diffusion chain to transform limited data into an expanded set of noised data. For class-level effectiveness, we design a two-branch generation structure that consists of a Diffusion-based Feature Generator (DFG) and a Diffusion-based Representation Generator (DRG). DFG focuses on learning and sampling the distribution of crossentropy-based features, whilst DRG learns the supervised contrastive-based representation to boost the zero-shot capabilities of DFG. Additionally, we employ three discriminators to evaluate generated features from various aspects and introduce a Wasserstein-distance-based mutual learning loss to transfer knowledge among discriminators, thereby enhancing guidance for generation. Demonstrated through extensive experiments on three popular ZSL benchmarks, our ZeroDiff not only achieves significant improvements over existing ZSL methods but also maintains robust performance even with scarce training data. Code will be released upon acceptance.

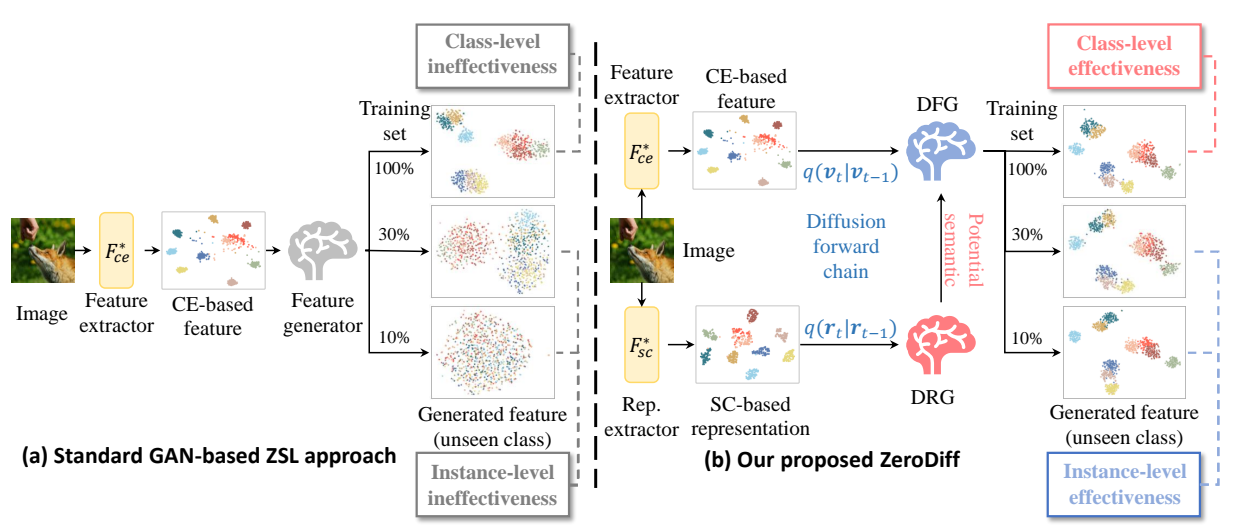


Fig. 1: Core idea of our ZeroDiff. (a) Standard GAN-based ZSL approaches suffer two problems in ZSL: (1) their performance drops when training data are decreased; and (2) they use incomplete pre-defined semantics to critic visual features. In contrast, our ZeroDiff leverages the diffusion noise process to obtain infinite noised real features for instance-level effectiveness; another diffusion-based representation generator is also used to get potential semantics for class-level effectiveness.

Keywords: Zero-shot Learning, Generative Model, Effective Learning, Deep Learning

## 1 Introduction

Machine learning models have achieved remarkable success in data-intensive applications, largely due to the availability of a huge number of labeled samples. However, as collecting such extensive labeled datasets is usually time-consuming and expensive, it is often unrealistic to assume that a large amount of labeled data is available. To address this limitation, researchers try to develop models which generalize well even in case of a limited number of samples. Among them, zero-shot learning (ZSL) (Chen et al, 2021a) stands out by separating categories into seen and unseen categories. During training, only image samples of the seen categories are accessible, while those of the unseen categories are reserved for testing. Generalized ZSL (GZSL) (Chao et al, 2016) reflects a more realistic scenario, where both seen and unseen categories are included in the testing phase.

To bridge the gap between seen and unseen classes, researchers have explored leveraging predefined semantic knowledge about classes such as attributes (Chao et al, 2016), text2vec (Zhu et al,

2018; Chen and Yeh, 2021), and DNA (Badirli et al, 2021). ZSL methods mainly follow two paths: embedding methods (Xu et al, 2020; Chen et al, 2022a; Ye et al, 2023) that learn direct mappings between visual and semantic modalities, and generative methods that use generative models such as GANs (Xian et al, 2018b; Li et al, 2021; Ye et al, 2021) and VAEs (Chen et al, 2021b,a) to synthesize data for unseen classes. Currently, ZSL methods with generative models have become a popular approach.

Despite rapid advances in ZSL, a common assumption is that a sufficient number of samples per *seen* class are available. In case of limited labeled data from each seen class, it remains uncertain if ZSL may still work, i.e. instance-level data effectiveness is not guaranteed. This oversight becomes apparent as few ZSL methods consider the case of limited or no samples during training (Verma et al, 2020; Gao et al, 2022; Tang et al, 2024). For example, a data-free ZSL method leverages the knowledge of CLIP (Tang et al, 2024) to demonstrate the potential of training without any real seen class data. However, this approach

does not conform to the universal evaluation protocols (Xian et al, 2018a), as the training of CLIP did not avoid using unseen classes in ZSL. In our experiments, we observe that most existing generative ZSL methods suffer from performance degradation and collapsed patterns when the number of training samples is gradually reduced. As shown in the t-SNE plot of Fig.1 (a), the classic method f-VAEGAN (Xian et al, 2019) drops the GZSL accuracy by 26.4% on 10% of the training data, compared to using all the training data. More results can be seen in Sec. 4.4.

To further address the data requirement challenges at both class and instance levels, we propose a diffusion-based generative ZSL model (ZeroDiff), which combines a diffusion model to generate more samples to address the identified limitations. As shown in Fig. 1 (b), our approach draws inspiration from the potential of diffusion models to improve instance effectiveness through a diffusion forward chain. Specifically, the original finite data is perturbed with different noise-to-data ratios, resulting in an infinite set of perturbed data points. In addition, to improve class effectiveness, we introduce a two-branch generation structure: diffusion-based feature generation (DFG) and diffusion-based representation generation (DRG) to distinguish it from traditional GAN-based methods. DFG is specifically designed to denoise visual features, transforming them from noise-enhanced to sharp states using predefined and potential semantics. These potential semantics come from frozen DRGs, which can capture a wider range of undefined semantics as they are trained on contrastive representations. In addition, we combine three types of discriminators to evaluate the authenticity of examples from various perspectives: predefined semantics, diffusion process, and contrastive representation. To promote mutual learning among all discriminators, we introduce a knowledge distillation loss based on Wasserstein distance, which further improves the model effectiveness.

Our contributions are multifaceted:

ZeroDiff paves the way for class- and instanceefficient ZSL via a novel diffusion generation
framework. To the best of our knowledge,
ZeroDiff is not only the first to apply generative diffusion models for zero-shot image
classification but also the first to explore
mutual learning of discriminators.

- We propose a novel mechanism to address instance-level overfitting via a forward diffusion chain in the diffusion model, where noise is mixed with clean samples in different proportions to avoid memorizing the training samples.
- We enhance the effectiveness of categories via a two-branch generation paradigm, which generates contrastive representations as potential semantics to help feature generation, thereby improving class-level effectiveness.
- We establish a new performance protocol to evaluate ZSL methods across varying data amounts, where experimental results demonstrate the superiority of ZeroDiff in both ZSL and GZSL settings.

## 2 Related Work

## 2.1 Zero-shot Learning

Zero-Shot Learning (ZSL) is an area of research focusing on class-level generalizability (Xian et al, 2018a). The primary approaches to ZSL can be categorized into embedding and generative methods. Embedding methods (Akata et al, 2015; Yang et al, 2016; Ding et al, 2017; Yang et al, 2016; Chen et al, 2022b; Ye et al, 2023) learn a direct mapping from visual to semantic spaces or vice versa. TransZero++ (Chen et al, 2022a) presents a transformer-based architecture into ZSL and introduced mutual learning (Zhang et al, 2018) to align the classification results of semantic and visual space. In case of a limited number of training samples, embedding methods often under-perform generative methods on smaller datasets (Chen et al, 2022b; Ye et al, 2023).

In contrast, generative ZSL methods employ a variety of generative models to synthesize images of unseen classes and then train a final classifier for these classes. There are also certain drawbacks for these methods. For example, GAN-based approaches frequently suffer from poor mode coverage (Nowozin et al, 2016; Arjovsky et al, 2017; Zhao et al, 2018), while VAE-based methods are plagued by low sample quality (Verma et al, 2018). To address these issues, some ZSL methods combine GANs and VAEs, such as f-VAEGAN (Xian et al, 2019) and TF-VAEGAN (Narayan et al, 2020). Furthermore, to compensate for the lack of discriminative power in predefined semantics, some

generative ZSL approaches incorporate contrastive learning or disentangled learning to uncover potential semantics, as seen in CEGAN (Han et al, 2021) and SDVAE (Chen et al, 2021b). However, these potential semantics are not directly used to generate images of unseen classes; they are only utilized for classifying test samples at test time.

## 2.2 Diffusion Models

Diffusion models (Sohl-Dickstein et al, 2015; Ho et al, 2020; Song et al, 2020a,b; Xiao et al, 2022) have a forward diffusion chain and a reverse denoising process. The forward diffusion chain gradually adds noise to the clean data  $\mathbf{x}_0 \sim q(\mathbf{x}_0)$  in T steps:

$$q(\mathbf{x}_{1:T}|\mathbf{x}_0) = \prod_{t \ge 1} q(\mathbf{x}_t|\mathbf{x}_{t-1}), \tag{1}$$

 $q(\mathbf{x}_t|\mathbf{x}_{t-1}) = \mathcal{N}(\mathbf{x}_t; \sqrt{1-\beta_t}\mathbf{x}_{t-1}, \beta_t \mathbf{I}),$ (2)where  $\beta_t$  is a pre-defined variance schedule. When t = T, the noised data  $\mathbf{x}_t$  becomes fully Gaussian noise. The reverse process leverages a denoising model G to remove noise from  $\mathbf{x}_t$ . The classical DDPM (Ho et al, 2020) designs three modes: (1) predicting noise added at t step, (2) predicting  $\mathbf{x}_{t-1}$ , and (3) predicting clean data  $\mathbf{x}_0$ (also called directly denoising), i.e.,  $p_G(\mathbf{x}_0|\mathbf{x}_t) =$  $p_{\mathbf{x}_0 \sim G(\mathbf{x}_t,t)}(\mathbf{x}_0|\mathbf{x}_t) = \mathcal{N}(\mathbf{x}_0;\boldsymbol{\mu}_{\theta},\boldsymbol{\sigma}_t^2\boldsymbol{I}).$  The third mode is also adopted in Denoising Diffusion GAN (DDGAN) (Xiao et al, 2022) that unifies diffusion model and GAN by utilizing a discriminator to implicitly learn the denoising goal that maximizes the likelihood  $p_G(\mathbf{x}_0) = \int p_G(\mathbf{x}_{0:T}) d\mathbf{x}_{1:T}$ .

Large-scale Diffusion Models: Recent works (Clark and Jaini, 2024; Li et al, 2023) have shown that large-scale diffusion models, such as the Latent Diffusion Model (also known as Stable Diffusion) (Rombach et al, 2022), have the ability to perform zero-shot classification. However, these studies do not strictly ensure that unseen classes are not used for model training. In these largescale diffusion studies, the zero-shot ability is more task-oriented. They primarily focus on the performance across various agnostic tasks and datasets. The assumption is that with sufficiently large training samples, good performance can be achieved for any task or dataset. In contrast, our work aims to improve effectiveness on small training sets. The concept of a "diffusion model" differs in this context. In prior works, a "diffusion model" refers to one or several specific pre-trained diffusion models. In this paper, our interpretation of a "diffusion model" is closer to its fundamental nature: a type of generative paradigm that learns the data distribution through denoising noised data. Our training strategy incorporates ideas from diffusion, but crucially, it does not violate the zero-shot premise.

We demonstrate the dramatic impact of the number of training samples to generative ZSL approaches. Additionally, our ZeroDiff introduces three innovations: (1) An integration of diffusion models to improve instance-level effectiveness. (2) A two-branch generation paradigm to improve class-level effectiveness. (3) A Wasserstein-distances-based loss to distill knowledge from multiple discriminators.

## 3 ZeroDiff

Our training algorithm contains three stages: (1) Fine-tuning stage by cross-entropy loss (CE) and supervised contrastive (SC) loss to extract visual features and contrastive representations; (2) Diffusion-based Representation Generator (DRG) training stage that models the contrastive representation distribution to support feature generation; (3) Diffusion-based Feature Generator (DFG) training stage that generates features conditioned by pre-defined semantics and contrastive representation. After training DFG and DRG, we use them to generate pseudo samples of unseen classes, and then utilize these generated samples to train our final ZSL/GZSL classifier. The whole training and testing algorithms can be found in the appendix.

## 3.1 Preliminary

In the ZSL setting, suppose there are two disjoint label sets: a seen set  $\mathcal{Y}^s$  used for training and an unseen set  $\mathcal{Y}^u$  used for testing, where  $\mathcal{Y}^s \cap \mathcal{Y}^u = \emptyset$ . We denote the training dataset as  $\mathcal{D}_{tr} = \{(x^s, y^s, a^s) \mid x^s \in \mathcal{X}^s, y^s \in \mathcal{Y}^s, a^s \in \mathcal{A}^s\}$ , where  $\mathcal{X}^s$ ,  $\mathcal{A}^s$ , and  $\mathcal{Y}^s$  represent the image, semantic, and label spaces corresponding to the seen classes. The goal of ZSL is to use the training dataset  $\mathcal{D}_{tr}$  to create a classifier that can classify unseen images in the testing dataset  $\mathcal{D}_{te}^u = \{(x^u, y^u, a^u) \mid x^u \in \mathcal{X}^u, y^u \in \mathcal{Y}^u, a^u \in \mathcal{A}^u\}$ , i.e.,  $f_{zsl}: \mathcal{X}^u \to \mathcal{Y}^u$ . In GZSL, we also need to classify images of seen classes during the testing stage. In other words,

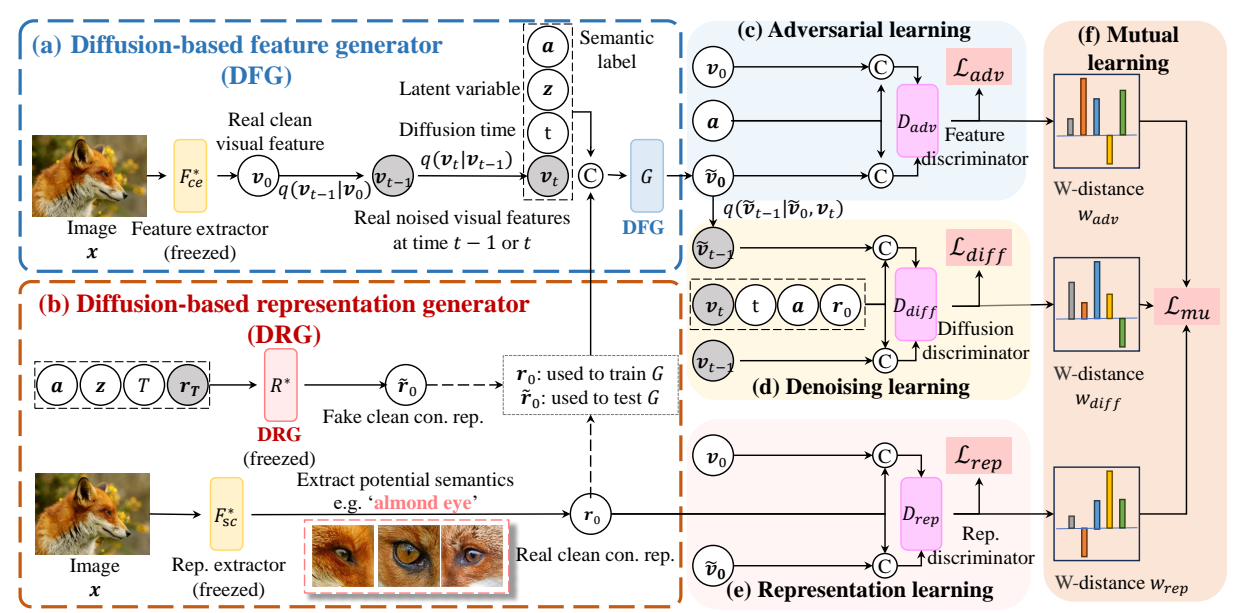
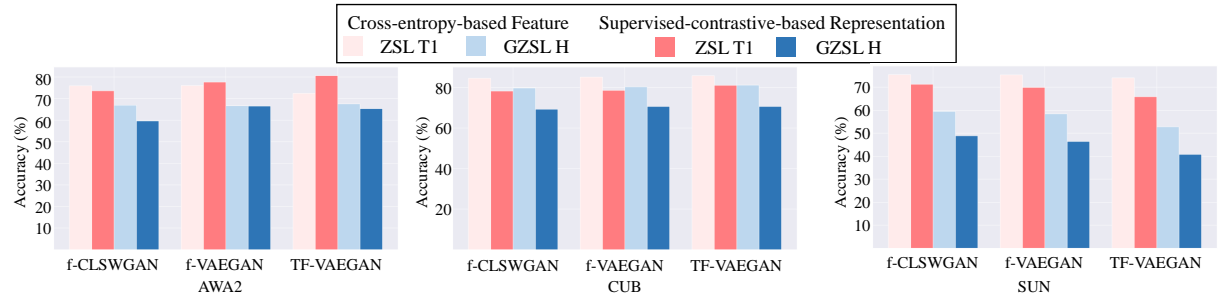


Fig. 2: The training pipeline of our DFG (the DRG training is similar) is as follows. © represents the concatenation operation. Given frozen extractors  $F_{ce}^*$  and  $F_{sc}^*$  (Sec. 3.2), we use them to extract clean visual features  $\mathbf{v}_0$  and contrastive representations  $\mathbf{r}_0$ . Then, we use the diffusion forward chain Eq. 1 to obtain real noised visual features  $\mathbf{v}_{t-1}$  and  $\mathbf{v}_t$ . Next, G in DFG denoises and generates a fake clean feature  $\tilde{\mathbf{v}}_0$ , conditioned by the concatenation of the semantic label  $\mathbf{a}$ , latent variable  $\mathbf{z}$ , diffusion time t, and noised feature  $\mathbf{v}_t$ . The fake clean feature is evaluated from three different learning perspectives: adversarial learning (Does it match predefined semantics?), denoising learning (Does it match diffusion processes?), and representation learning (Does it match contrastive representations?). Finally, we present the mutual learning loss  $\mathcal{L}_{mu}$  to integrate the three discriminators.



**Fig. 3**: Comparison of performance between CE-based features and SC-based representations. We selected three typical generative ZSL methods to evaluate these two fine-tuning losses. We found that CE is better than SC in most cases, except for the ZSL T1 accuracy in AWA2.

the testing dataset becomes  $\mathcal{D}_{te} = \mathcal{D}_{te}^s \cup \mathcal{D}_{te}^u$ , and the goal becomes  $f_{qzsl} : \mathcal{X}^s \cup \mathcal{X}^u \to \mathcal{Y}^s \cup \mathcal{Y}^u$ .

## 3.2 Fine-Tuning Extractor

Before we start our diffusion-based generation, we want to emphasize the importance of our fine-tuning stage. Previously, many ZSL works, e.g., (Han et al, 2021), generally assume that Supervised Contrastive (SC) learning can produce more discriminative representations than those extracted using Cross-Entropy (CE). However, other influential works have shown that representations learned from SC are more sensitive to data imbalance (Cui

et al, 2021; Jiang et al, 2021; Zhu et al, 2022; Cui et al, 2023). Fewer training samples lead to poorer SC-trained representations. Thus, because unseen classes have no samples for SC training, we raise the question: Is SC really better than CE for ZSL?

To explore this question, we selected ResNet101 (He et al, 2016) as the extractor, which is the most widely-used architecture in ZSL. We used SC and CE to pretrain two ResNet101 models on ImageNet, respectively. We define the CE-pretrained model as  $F_{ce}$  and the SC-pretrained model as  $F_{sc}$ . Next, we used CE and SC to fine-tune these models on the ZSL training set  $\mathcal{D}_{tr}$ , and then froze them as  $F_{ce}^*$  and  $F_{sc}^*$ . Finally, we used traditional generative ZSL approaches to evaluate the ZSL performance of SC-based representations and CE-based features. We found that SC performance is generally worse significantly compared to that of traditional CE. The results can be found in Fig. 3.

## 3.3 Diffusion-based Representation Generator

Although directly using SC-based representations for classification is not better than using CE-based features for ZSL, existing work has shown that contrastive losses enjoy the ability to capture potential semantics (Islam et al, 2021; Ye et al, 2021; Li et al, 2024). For example, as shown in Fig. 2 (b), the 'almond eye' is a significant semantic feature of the fox class. However, the AWA2 dataset does not contain this key semantic annotation. In fact, relying solely on predefined semantics to cover all true semantics is impracticable.

In this work, we leverage SC-based representations to mine potential semantics and address the incompleteness of predefined semantics<sup>1</sup>. As shown in Fig. 2, DFG generates visual features from limited data, while DRG aims to enhance the potential semantics to support the DFG. We train the DRG and freeze it before training the DFG. They have the same training procedure, differing only in their input, output, and corresponding discriminators. Thus, in the following, we only describe the DFG

training, as it is more complicated. More details can be found in the appendix.

## 3.4 Diffusion-based Feature Generator

Given an image  $x^s$  from the training set  $\mathcal{D}_{tr}$ , we use the fine-tuned  $F_{ce}^*$  and  $F_{sc}^*$  to extract its clean visual features  $\mathbf{v}_0 = F_{ce}^*(x^s)$  and clean contrastive representation  $\mathbf{r}_0 = F_{sc}^*(x^s)$ . Next, following previous diffusion models (Ho et al, 2020; Xiao et al, 2022), we adopt the diffusion noising process to obtain infinite data at multiple noise levels from weak to strong according to the diffusion forward chain in Eq. 1. We set the maximum diffusion time as T and randomly sample a diffusion time  $t \sim U(1, \cdots, T)$ . We denote the noised visual features as  $\mathbf{v}_{t-1}$  and  $\mathbf{v}_t$  at the diffusion times t-1 and t, respectively. Next, to model the denoising process, we concatenate the noised feature  $\mathbf{v}_t$ , diffusion time t, predefined class semantics  $\mathbf{a}$ , latent variable  $\mathbf{z}$ , and contrastive representation  $\mathbf{r}_0$  as the input of G, that is,  $\tilde{\mathbf{v}}_0 = G(\mathbf{a}, \mathbf{r}_0, t, \mathbf{v}_t, \mathbf{z})$ . After denoising/generating a clean feature  $\tilde{\mathbf{v}}_0$ , it is evaluated from three aspects: adversarial learning, denoising learning, and representation learning.

Adversarial Learning: First, as shown in Fig. 2(c), we follow the standard WGAN (Arjovsky et al, 2017) and WGAN-GP (Gulrajani et al, 2017) and train a discriminator  $D_{adv}$  that distinguishes clean real features  $\mathbf{v}_0$  from fake features  $\tilde{\mathbf{v}}_0$  by predicting the Wasserstein distance  $W_{adv}$  between them according to predefined semantics a. Specifically, the discriminator  $D_{adv}$  maximizes the following loss  $\mathcal{L}_{adv}$ :

$$\mathcal{L}_{adv} = W_{adv} - \lambda_{qpadv} \mathcal{L}_{qpadv}, \tag{3}$$

$$W_{adv} = \mathbb{E}[D_{adv}(\mathbf{v}_0, \mathbf{a})] - \mathbb{E}[D_{adv}(\tilde{\mathbf{v}}_0, \mathbf{a})], \quad (4)$$

$$\mathcal{L}_{gpadv} = \mathbb{E}[(\|\nabla_{\hat{\mathbf{v}}_0} D_{adv}(\hat{\mathbf{v}}_0, \mathbf{a})\|_2 - 1)^2], \quad (5)$$

where  $\hat{\mathbf{v}}_0 = \alpha \mathbf{v}_0 + (1 - \alpha)\tilde{\mathbf{v}}_0$  with  $\alpha \sim U(0, 1)$ , and  $\lambda_{gpadv}$  is a coefficient of the gradient penalty term  $\mathcal{L}_{gpadv}$  (Gulrajani et al, 2017) that makes GANs training more stable.

**Denoising Learning:** Second, as mentioned, due to the limited number of training examples,  $D_{adv}$  can easily overfit to the limited training

<sup>&</sup>lt;sup>1</sup>Previous ZSL work, e.g., (Han et al, 2021; Chen et al, 2021b), has also explored the power of potential semantics in ZSL. However, most of them only use potential semantics for classifying test samples. Our designed two-branch generation paradigm helps both the final classification and feature generation.

features. To address this, we design the diffusion discriminator  $D_{diff}$  to alleviate such instance overfitting, as shown in Fig. 2(d).  $D_{diff}$  needs to approximate the true denoising distribution  $q(\mathbf{v}_{t-1}|\mathbf{v}_t)$ . To this end, we posterior-sample the real noised visual feature  $\mathbf{v}_{t-1}$  as well as the fake noised visual feature  $\tilde{\mathbf{v}}_{t-1}$ :

$$\tilde{\mathbf{v}}_{t-1} \sim q(\tilde{\mathbf{v}}_{t-1}|\tilde{\mathbf{v}}_0, \mathbf{v}_t) = \mathcal{N}(\tilde{\mathbf{v}}_{t-1}; \tilde{\mu}_t(\mathbf{v}_t, \tilde{\mathbf{v}}_0), \tilde{\beta}_t \mathbf{I}),$$
(6)

$$\tilde{\mu}_t(\mathbf{v}_t, \mathbf{v}_0) = \frac{\sqrt{\bar{\alpha}_{t-1}}\beta_t}{1 - \bar{\alpha}_t}\mathbf{v}_0 + \frac{\sqrt{\alpha_t}(1 - \bar{\alpha}_{t-1})}{1 - \bar{\alpha}_t}\mathbf{v}_t,$$
(7)

$$\tilde{\beta}_t = \frac{1 - \bar{\alpha}_{t-1}}{1 - \bar{\alpha}_t} \beta_t, \quad \bar{\alpha}_t = \prod_{j=1}^t (1 - \beta_j).$$
 (8)

Then, we train  $D_{diff}$  to learn the Wasserstein distance between them:

$$\mathcal{L}_{diff} = W_{diff} - \lambda_{qpdiff} \mathcal{L}_{qpdiff}, \qquad (9)$$

$$W_{diff} = \mathbb{E}[D_{diff}(\mathbf{v}_{t-1}, \mathbf{v}_t, \mathbf{r}_0, \mathbf{a}, t)] - \mathbb{E}[D_{diff}(\tilde{\mathbf{v}}_{t-1}, \mathbf{v}_t, \mathbf{r}_0, \mathbf{a}, t)], \quad (10)$$

$$\mathcal{L}_{gpdiff} = \mathbb{E}[(\|\nabla_{\hat{\mathbf{v}}_{t-1}} D_{diff}(\hat{\mathbf{v}}_{t-1}, \mathbf{v}_t, \mathbf{r}_0, \mathbf{a}, t)\|_2 - 1)^2],$$
(11)

where  $\hat{\mathbf{v}}_{t-1} = \alpha \mathbf{v}_{t-1} + (1-\alpha)\tilde{\mathbf{v}}_{t-1}$  with  $\alpha \sim U(0,1)$ . Our G minimizes  $\mathcal{L}_{gpdiff}$ , which equates to minimizing the learned divergence per denoising step:

$$\sum_{t>1} \mathbb{E}[D_{diff}(q(\mathbf{v}_{t-1}|\mathbf{v}_t)) \| p_G(q(\tilde{\mathbf{v}}_{t-1}|\mathbf{v}_t))]. \quad (12)$$

**Representation Learning:** Third, the representation discriminator  $D_{rep}$  is responsible for distinguishing features via contrastive representation view. It operates in a similar manner to  $D_{adv}$ , but with the predefined semantics **a** replaced by the contrastive representation, i.e.,

$$\mathcal{L}_{rep} = W_{rep} - \lambda_{qprep} \mathcal{L}_{qprep}, \tag{13}$$

$$W_{rep} = \mathbb{E}_{q(\mathbf{v}_0)}[D_{rep}(\mathbf{v}_0, \mathbf{r}_0)] - \mathbb{E}_{p_G(\tilde{\mathbf{v}}_0)}[D_{rep}(\tilde{\mathbf{v}}_0, \mathbf{r}_0)], \tag{14}$$

$$\mathcal{L}_{gprep} = \mathbb{E}_{\substack{q(\mathbf{v}_0), \\ p_G(\tilde{\mathbf{v}}_0)}} [(\|\nabla_{\hat{\mathbf{v}}_0} D_{rep}(\hat{\mathbf{v}}_0, \mathbf{r}_0)\|_2 - 1)^2].$$

$$\tag{15}$$

Mutual Learning: Since our three discriminators evaluate features in different ways, they have different criteria for judging them. If we can enable them to learn mutually, we can obtain stronger discriminators, resulting in better guidance for the generator. For example, the objectives of  $D_{adv}$  and  $D_{diff}$  are two very similar but distinct tasks: one separates clean features and the other separates noised features. Clearly, separating noised features is a harder task because with more diffusion steps, less information remains. Thus, if we can distill the knowledge from  $D_{adv}$  to  $D_{diff}$ , we can enhance the separation ability on noised features and use the stronger  $D_{diff}$  to improve denoising. In contrast, distilling the knowledge from  $D_{diff}$  to  $D_{adv}$  could prevent  $D_{adv}$  from memorizing training samples.

To unify their critiques about the same visual features, we propose our Wasserstein-distance-based knowledge distillation loss:

$$\mathcal{L}_{mu} = \kappa_t^{\gamma} * (\|W_{diff} - W_{adv}\|_1 + \|W_{diff} - W_{rep}\|_1) + \|W_{adv} - W_{rep}\|_1, \tag{16}$$

where  $\kappa_t$  is the Noise-to-Data (N2D) ratio, represented as  $1-\sqrt{\prod_{j=1}^t(1-\beta_j)}$ , and  $\gamma$  is a smoothing factor. As t increases,  $\kappa_t$  also increases, making it harder to distinguish between fake and real noised features, and  $W_{diff}$  provides less guidance for  $W_{rep}$  and  $W_{adv}$ . Therefore, we introduce a smoothing factor  $\gamma \geq 0$  to control the strength of discriminator alignment.

## 3.5 Optimization

The ZeroDiff model alternately trains G and three discriminators  $D_{adv}$ ,  $D_{diff}$ , and  $D_{rep}$  to optimize the following objective function:

$$\min_{G} \max_{D_{adv}, D_{diff}, D_{rep}} (\mathcal{L}_{adv} + \mathcal{L}_{diff} + \mathcal{L}_{rep} - \lambda_{mu} \mathcal{L}_{mu}),$$
(17)

where  $\lambda_{mu}$  is the hyper-parameter related to the mutual learning. After completing the training, we freeze them and denote them as  $R^*$  and  $G^*$ .

## 3.6 ZSL Inference

Finally, we use the ZeroDiff model to train the final ZSL classifier, i.e., for ZSL inference. Since multimodal feature spaces show stronger discriminative power (Narayan et al, 2020; Wang et al, 2023; Ye et al, 2021), we use frozen  $F_{ce}^*$  and  $F_{sc}^*$  to project the test samples into the visual feature space  $\mathcal{V}^u$  and representation space  $\mathcal{C}^u$ . Then, we use the frozen  $R^*$  to sample contrastive representations and feed them into the frozen  $G^*$  to synthesize visual features  $\tilde{\mathbf{x}}_0^u$  of unseen classes (generating  $N_{syn}$  samples for each unseen class). Next, we train the final classifier  $F_{zsl}$ , i.e.  $\mathcal{X}^u \to \mathcal{V}^u \to \mathcal{Y}^u$ .

# 4 Experiments

#### 4.1 Dataset Details

We conduct our experiments on three popular ZSL benchmarks: AWA2 (Xian et al, 2018a), CUB (Welinder et al, 2010) and SUN (Patterson and Hays, 2012). AWA2 has 65 animal classes with 85-D attributes and includes and 37322 images. CUB is a bird dataset containing 11788 images of 200 bird species. SUN have 14340 images of 645 seen and 72 unseen classes of scenes. We follow the commonly used setting (Xian et al, 2018a) to split seen and unseen classes. We report the average per-class Top-1 accuracy of unseen classes for ZSL. For GZSL, we evaluate the Top-1 accuracy on seen classes (S) and unseen classes (S), and report their harmonic mean S0 and S1 and S2 and S3 and S3 and S4 and S5 and S5 and S5 and S6 and S6 and S7 and S8 are classes (S9 and unseen classes (S9), and report their harmonic mean S9 and S9 are classes (S9 and unseen classes (S9).

Implementation Details. For visual features, we extract 2048-D features for all datasets using ResNet-101 (He et al., 2016) pre-trained with cross-entropy on ImageNet-1K (Deng et al, 2009). For contrastive representations, we adopt ResNet-101 pre-trained with PaCo (Cui et al, 2021) on ImageNet-1K. For semantic labels, we use attribute vectors for AWA2 and 1024-D attributes extracted from textual descriptions (Reed et al, 2016) for CUB and SUN. We use the Adam to optimize all networks with an initial learning rate of 0.0005. For all datasets,  $\lambda_{gpadv}$ ,  $\lambda_{gpdiff}$ , and  $\lambda_{gprep}$  are fixed at 10, and the number of diffusion steps T is set to 4, following DDGAN (Xiao et al, 2022). To compute  $\beta_t$  in Eq. 1, we use the discretization of the continuous-time extension, known as the Variance Preserving (VP) SDE (Song et al, 2020b). All experiments conducted in Quadro RTX 8000. The random seed are fixed to 9182, 3483 and 4115 for AWA2, CUB and SUN, respectively.

## 4.2 Comparison with State-of-the-art

representative We select generative ZSL methods across different generative model types. These methods include: 1. based methods: f-CLSWGAN (Xian et al, 2018b), CEGAN (Han et al, 2021) and CMC-GAN (Yang et al, 2023) 2. VAE-based methods: SDVAE (Chen et al, 2021b) 3. VAEGANbased methods: f-VAEGAN (Xian et al, TFVAEGAN (Narayan et al, 2020), APN+TFVAEGAN (Xu et al, 2022) 4. Flowbased method: DFCAFlow (Su et al, 2023). For fair comparisons, we reproduce some methods whose code is available with our *fine-tuned* features and the recommended hyperparameters (e.g., learning rate, number of synthesized unseen features, batch size) from their respective papers. Additionally, since generative approaches are trained with fine-tuned features, we can also directly compare them to embedding-based SOTA approaches: APN (Xu et al, 2020), TransZero++ (Chen et al, 2022b), I2DFormer (Naeem et al, 2022), MSDN (Chen et al, 2022c), PSVMA (Liu et al, 2023), ReZSL (Ye et al, 2023) and IAB (Jiang et al. 2024).

The ZSL results are in Table 1 and GZSL results are in Table 2. It can be observed from Table 1 that, in general, the proposed ZeroDiff outperforms the SOTAs, particularly in AWA2. For ZSL, the new SOTA performance that we have achieved is 86.4% (AWA2), 87.5% (CUB), and 77.3% (SUN), surpassing the second best methods by 10.5% (fCLSWGAN in AWA2), 1.7% (TFVAE-GAN in CUB) and 0.1% (DFCAFlow in SUN). For GZSL, our ZeroDiff still is excellently good at AWA2 and CUB, our *H* performances are 79.5% and 81.6% while the second bests are only 73.7% and 81.1%.

## 4.3 Ablation Study

## 4.3.1 Component Effectiveness

We examine the effect of the proposed components: G, R,  $D_{adv}$ ,  $D_{diff}$ ,  $D_{rep}$ , and  $\mathcal{L}_{mu}$ . The results are reported in Table 3. We observe that  $D_{diff}$  and  $\mathcal{L}_{mu}$  consistently improve performance across the three datasets. Another observation is that,

**Table 1**: Comparisons with the state-of-the-art on standard ZSL. We represent the top-1 accuracy (%) of unseen classes. The best and second-best results are marked in **Red** and **Blue**, respectively. † denoted the results using our fine-tune features.

Method	Reference	AWA2	CUB	SUN
APN (Xu et al, 2020)	NeurIPS20	68.4	72.0	61.6
I2DFormer (Naeem et al, 2022)	NeurIPS22	76.4	45.4	-
MSDN (Chen et al, 2022c)	CVPR22	70.1	76.1	65.8
TransZero++ (Chen et al, 2022a)	TPAMI22	72.6	78.3	67.6
ReZSL (Ye et al, 2023)	TIP23	70.9	80.9	63.0
IAB (Jiang et al, 2024)	IJCV24	74.5	78.0	65.7
fCLSWGAN (Xian et al, 2018b) <sup>†</sup>	CVPR18	75.9	84.5	75.5
f-VAEGAN (Xian et al, 2019) †	CVPR19	75.8	85.1	75.4
TFVAEGAN (Narayan et al, 2020) <sup>†</sup>	ECCV20	72.4	85.8	74.1
SDVAE (Chen et al, 2021b) <sup>†</sup>	ICCV21	69.3	85.1	77.0
CEGAN (Han et al, 2021)†	CVPR21	72.8	84.6	74.1
APN+TFVAEGAN (Xu et al, 2022)	IJCV22	73.5	74.7	66.3
DFCAFlow (Su et al, 2023) <sup>†</sup>	TCSVT23	74.4	83.9	77.2
CMC-GAN (Yang et al, 2023)	IJCV23	-	61.4	63.7
${f ZeroDiff}^\dagger$	Ours	86.4	87.5	77.3

**Table 2**: Comparisons with the state-of-the-art on standard GZSL. U, S, and H represent the top-1 accuracy (%) of unseen classes, seen classes, and their harmonic mean, respectively. The best and second-best results are marked in **Red** and **Blue**, respectively. † denoted the results using our fine-tune features.

Method	Reference		AWA2			CUB			SUN		
Method	Tererence	U	S	Н	U	S	Н	U	S	Н	
APN	NeurIPS20	57.1	72.4	63.9	65.3	69.3	67.2	41.9	34.0	37.6	
I2DFormer	NeurIPS22	66.8	76.8	71.5	35.3	57.6	43.8	-	-	-	
MSDN	CVPR22	62.0	74.5	67.7	68.7	67.5	68.1	52.2	34.2	41.3	
TransZero++	TPAMI22	64.6	82.7	72.5	67.5	73.6	70.4	48.6	37.8	42.5	
PSVMA	CVPR23	73.6	77.3	75.4	70.1	77.8	73.8	61.7	45.3	52.3	
ReZSL	TIP23	63.8	85.6	73.1	72.8	74.8	73.8	47.4	34.8	40.1	
IAB	IJCV24	70.0	83.8	76.3	70.1	78.5	74.0	46.9	42.7	44.7	
fCLSWGAN <sup>†</sup>	CVPR18	65.1	68.9	66.9	76.4	83.3	79.7	63.8	55.7	59.5	
$ ext{f-VAEGAN}^\dagger$	CVPR19	67.3	65.6	66.4	77.4	83.5	80.3	63.6	54.1	58.4	
$\mathrm{TFVAEGAN}^{\dagger}$	ECCV20	54.2	89.6	67.5	79.0	83.3	81.1	51.8	53.8	52.8	
$\mathrm{SDVAE}^\dagger$	ICCV21	57.0	72.3	63.8	81.6	74.2	77.7	62.3	56.9	59.5	
$CEGAN^{\dagger}$	CVPR21	57.1	89.0	69.6	78.9	80.9	79.9	58.1	57.4	57.8	
APN+TFVAEGAN	IJCV22	60.9	79.1	68.8	65.6	76.3	70.6	52.6	37.3	43.7	
$\mathrm{DFCAFlow}^\dagger$	TCSVT23	<b>67.6</b>	81.0	<b>73.7</b>	77.3	82.9	80.0	63.0	<b>59.6</b>	61.2	
CMC-GAN	IJCV23	-	-	-	52.6	65.1	58.2	48.2	40.8	44.2	
$\mathbf{ZeroDiff}^{\dagger}$	Ours	74.7	85.0	<b>79.5</b>	80.0	83.2	81.6	63.0	<b>56.9</b>	<b>59.8</b>	

in many cases, G benefits from the inclusion of R, although R does not perform better than G alone. It also is a evidence for our motivation that SC-based representations could capture potential features to support features generation.

### 4.3.2 Hyper-parameter Sensitivity

We also provide the hyper-parameter sensitivity analysis for the number of generated samples per unseen class  $N_{syn}$  and the factor  $\gamma_{mu}$  that controls the smoothing of the noise-to-data ratio (Eq. 16).

**Table 3**: Ablation study of our ZeroDiff. In ZSL, T1 represents the top-1 accuracy (%) of unseen classes. In GZSL, U, S, and H represent the top-1 accuracy (%) of unseen classes, seen classes, and their harmonic mean, respectively.  $\checkmark$  and  $\times$  denote yes and no.  $\bigcirc$  denotes using corresponding versions for DRG.

Component					AW	AWA2		CUB		SUN	
$\overline{G}$	R	$D_{adv}$	$D_{diff}$	$D_{rep}$	$\mathcal{L}_{mu}$	T1	Н	T1	Н	T1	Н
	×	✓	×	×	×	79.9	67.0	83.7	78.5	74.7	57.8
$\checkmark$	×	$\checkmark$	$\checkmark$	×	×	82.3	72.9	84.1	79.5	75.1	58.7
×	$\checkmark$	$\circ$	$\circ$	×	×	83.8	67.1	78.3	66.8	71.6	47.6
$\checkmark$	$\checkmark$	$\checkmark$	$\checkmark$	$\checkmark$	×	84.6	77.5	84.8	79.3	76.8	59.2
$\checkmark$	$\checkmark$	$\checkmark$	$\checkmark$	$\checkmark$	$\checkmark$	86.4	79.5	87.5	80.3	77.3	59.8

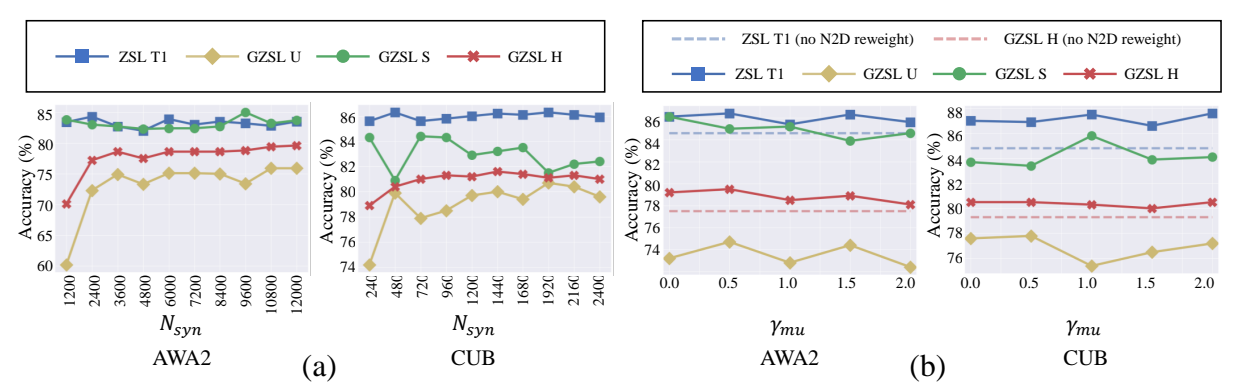


Fig. 4: Hyper-parameter Sensitivity. (a) The effect of the number of synthetic samples  $N_{syn}$ . (b) The effect of  $\gamma_{mu}$  that controls the smoothing of N2D reweight  $\kappa_t^{\gamma_{mu}}$  (Eq.16).

Results are shown in Fig. 4. From Fig. 4 (a), we can see that a small  $N_{syn}$  might undermines GZSL performance, but with  $N_{syn}$  increasing, the GZSL performance tends to stabilization. From Fig. 4 (b), we can find our method perform robust for the change of  $\gamma_{mu}$ , and with N2D reweight is consistently better than the counterpart that without N2D reweight.

## 4.4 Limited Training Data

To investigate the performance of generative ZSL approaches under limited training data, we randomly keep training samples of each seen class by different ratios. As the remaining ratio decreases, ZSL becomes more challenging since overfitting to the training samples becomes much easier. For fairness, we decrease the number of synthesized unseen features proportionally to avoid class imbalance in GZSL. The full set of hyperparameters can be found in the appendix. The results are reported in Table 4.

The following observations can be made: <u>First</u>, GAN-based approaches, f-VAEGAN and CEGAN, deteriorate severely when only limited training data is available. This indicates that GANs are fragile under limited data conditions. <u>Second</u>, the semantic rectification methods, SDVAE and DFCAFlow, maintain relatively good accuracy. This suggests that semantic rectification is also an effective way to avoid overfitting with limited training data. <u>Third</u>, with the introduction of diffusion models, our ZeroDiff achieves the best performance in many cases. This demonstrates the effectiveness of our method in improving data efficiency.

We also provide a qualitative comparison between the baseline f-VAEGAN and our ZeroDiff using t-SNE visualization of the real and synthesized sample features in Fig. 5. The visualization shows that as the number of training samples decreases, f-VAEGAN gradually fails to generate unseen classes, while our ZeroDiff maintains a highly robust ability to generate them.

**Table 4**: Comparison on limited training data. We evaluate generation methods with 30% and 10% training samples. T1 represents the top-1 accuracy (%) of unseen classes in ZSL. In GZSL, U, S, and H represent the top-1 accuracy (%) of unseen classes, seen classes, and their harmonic mean, respectively. The best and second-best results are marked in **Red** and **Blue**, respectively.

	AWA2				CUB				SUN			
Method	30%		10%		30%		10%		30%		10%	
	T1	Н	T1	Н	T1	Н	T1	Н	T1	Н	T1	Н
f-VAEGAN (Xian et al, 2019)	76.6	55.0	65.1	40.0	82.1	75.3	74.7	66.4	73.4	51.5	66.9	29.3
SDVAE (Chen et al, 2021b)	70.9	66.6	62.4	45.8	82.7	77.2	84.3	77.5	<b>75.8</b>	<b>52.6</b>	<b>70.0</b>	34.4
CEGAN (Han et al, 2021)	72.2	70.4	69.0	66.3	83.6	<b>77.6</b>	81.3	74.8	65.9	45.6	-	-
DFCAFlow (Su et al, 2023)	74.5	<b>72.6</b>	<b>77.9</b>	70.7	82.7	77.2	80.3	74.1	74.2	55.8	70.2	31.3
ZeroDiff (Ours)	84.9	80.2	83.3	<b>77.0</b>	85.5	<b>78.7</b>	82.9	<b>76.1</b>	<b>75.4</b>	51.3	68.1	33.3

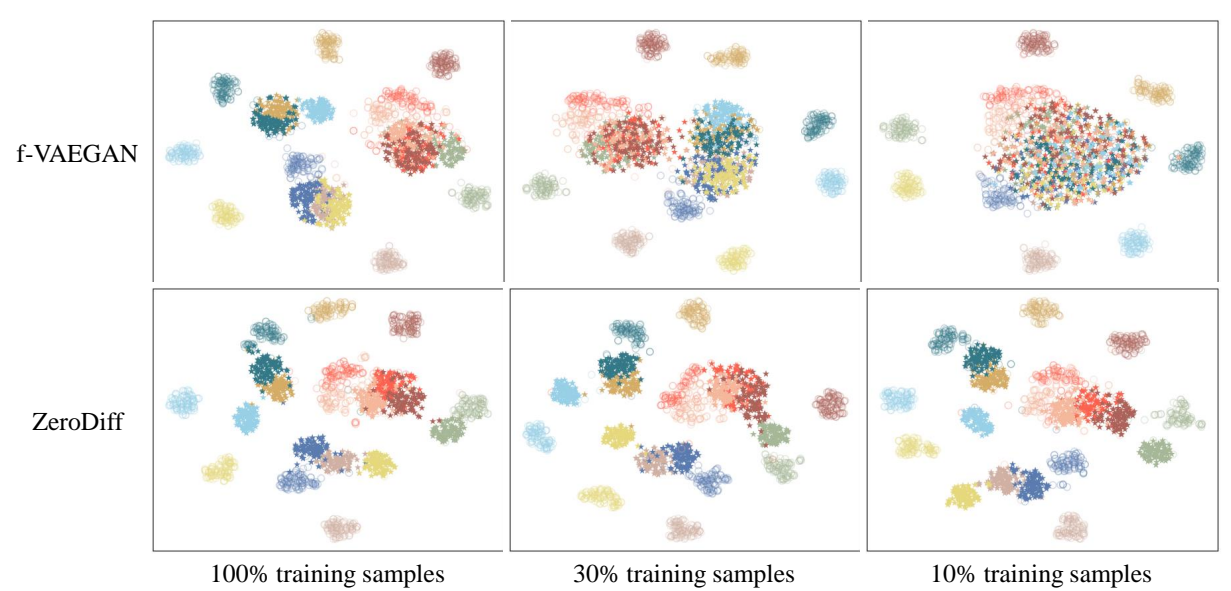


**Fig. 5**: Qualitative evaluation with t-SNE visualization on AWA2. We randomly selected 100 generated samples per class and all real samples for 10 unseen classes. We use different colors to denote classes, and use ∘ and ∗ to denote the real and synthesized sample features, respectively (Best Viewed in Color).

## 4.5 DDGAN v.s. ZeroDiff

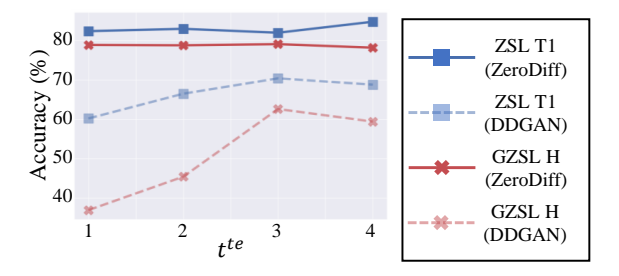
We also compare ZeroDiff to DDGAN, a similar work combining GAN and diffusion models. Since both methods are based on diffusion, we can control the number of denoising/generating steps  $t^{te}$  during testing. The results are reported in Fig. 6.

We find that DDGAN requires multiple steps to achieve good generation/denoising performance, while our ZeroDiff performs consistently well across different denoising iterations. Thus, we can denoise/generate fake data by only one-step

at inference stage and do not reduce generation performance.

## 4.6 Mutual Learning Effectiveness

To further verify the effect of our  $\mathcal{L}_{mu}$ , we designed an additional experiment to show the change in critic score. Generally, a higher critic score means that discriminators consider the input data more realistic, and vice versa. <u>First</u>, as shown in Fig. 7 (a), we display the critic score difference of the discriminator  $D_{adv}$  between clean real training features  $\mathbf{v}_0^{tr}$  and test features  $\mathbf{v}_0^{te}$  of **seen classes** 



Varying test denoising time  $t^{te}$  effect.

Fig. 6: Comparing ZeroDiff to DDGAN.

under the GZSL setting, i.e.,

$$\Delta_{adv}(\mathbf{v}_0^{tr}, \mathbf{v}_0^{te}) = D_{adv}(\mathbf{v}_0^{tr}, \mathbf{a}^{tr}) - D_{adv}(\mathbf{v}_0^{te}, \mathbf{a}^{te}).$$
(18)

A larger  $\Delta_{adv}$  indicates that  $D_{adv}$  considers real test samples more likely to be fake, indicating memorization of limited real training samples. With  $\mathcal{L}_{mu}$ ,  $\Delta_{adv}$  decreases significantly compared to the counterpart without  $\mathcal{L}_{mu}$  in CUB and SUN, suggesting that knowledge from  $D_{diff}$  helps  $D_{adv}$  reduce overfitting in the training set. <u>Second</u>, conversely, the knowledge from  $D_{adv}$  can also benefit  $D_{diff}$ . As shown in Fig. 7 (b), we display the critic score difference of  $D_{diff}$  between noised real training features  $\mathbf{v}_t^{tr}$  and noised fake training features  $\tilde{\mathbf{v}}_t^{tr}$ , i.e.,

$$\Delta_{diff}(\mathbf{v}_t^{tr}, \tilde{\mathbf{v}}_t^{tr}) = D_{diff}(\mathbf{v}_t^{tr}, \mathbf{v}_{t+1}^{tr}, \mathbf{r}_0^{tr}, \mathbf{a}^{tr}, t) - D_{diff}(\tilde{\mathbf{v}}_t^{tr}, \mathbf{v}_{t+1}^{tr}, \mathbf{r}_0^{tr}, \mathbf{a}^{tr}, t).$$
(19)

After adding  $\mathcal{L}_{mu}$ ,  $\Delta_{diff}$  increases significantly. This indicates that the distinguishing ability of  $D_{diff}$  is enhanced by the knowledge from  $D_{adv}$ .

## 5 Conclusion

In this study, we explore the Zero-Shot Learning (ZSL) problem in scenarios with limited seen data and propose a data-efficient ZSL method based on a diffusion generative model. We enhance the training samples using a diffusion forward chain and adopt contrastive representation to support feature generation, significantly improving zero-shot capacity with both sufficient and limited training

samples. Additionally, our proposed mutual learning loss, based on Wasserstein distance, allows different discriminators to learn from each other. Experiments on three popular datasets demonstrate the data efficiency of our method, showcasing its robustness in cases with both ample and limited training data.

Acknowledgements. This work was partially supported by Research Development Fund with No. RDF-22-01-020 and "Qing Lan Project" in Jiangsu universities, National Natural Science Foundation of China under No. U1804159, and Jiangsu Science and Technology Programme under No. BE2020006-4

## **Declarations**

- Funding: Research Development Fund with No. RDF-22-01-020. National Natural Science Foundation of China (No. U1804159). Jiangsu Science and Technology Programme (No. BE2020006-4).
- Conflict of interest: The authors declare that they have no known competing financial interests or personal relationships that could have appeared to influence the work reported in this paper.

Data Availability Statement. The AWA2, CUB and SUN datasets are publicly available at http://cvml.ist.ac.at/AwA2/, https://www.vision.caltech.edu/datasets/cub\_200\_2011/ and https://cs.brown.edu/~gmpatter/sunattributes.html, respectively. The models and source data generated during and analyzed during the current study are available from the corresponding author upon reasonable request.

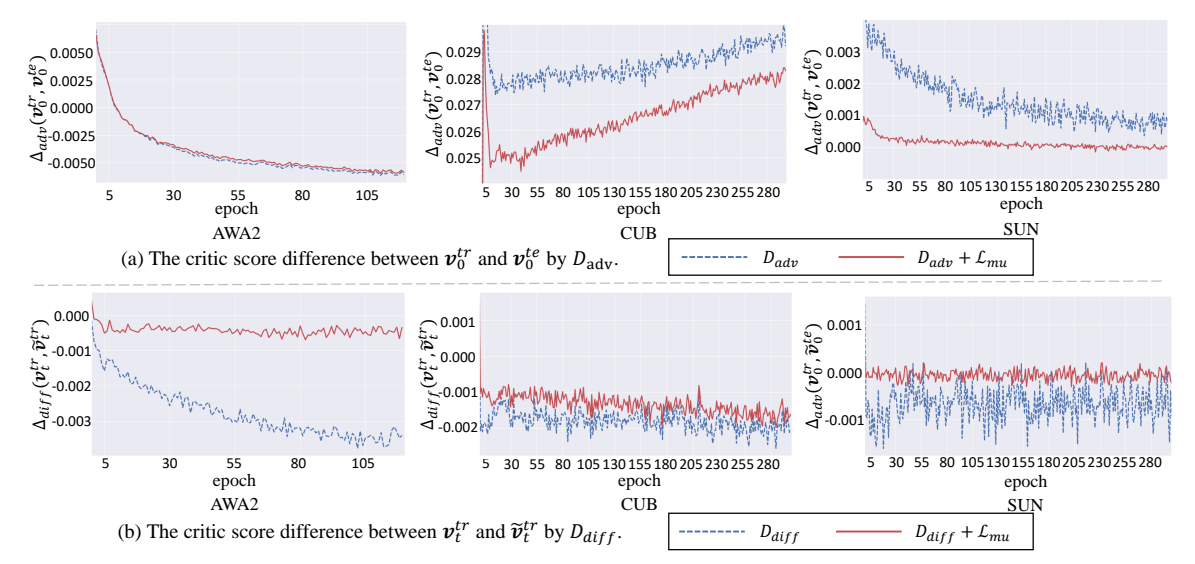


**Fig. 7**: The effect of  $\mathcal{L}_{mu}$  to  $D_{adv}$  and  $D_{diff}$ . (a) indicates that our  $\mathcal{L}_{mu}$  mitigates the overfitting of  $D_{adv}$  in the training set. (b) shows that the distinguishing ability of  $D_{diff}$  is enhanced by our  $\mathcal{L}_{mu}$  across different datasets.

# Appendix A Algorithms

We include here pseudo-code for training algorithms (Alg.1 and Alg.2) and testing algorithm (Alg. 3). We also discuss used losses not covered before here:

#### Fine-tuning stage:

For the feature extractor  $F_{ce}$ :

$$\mathcal{L}_{CE} = -\sum_{i=1}^{\|\mathcal{Y}\|} \mathbf{y}_i \log(\widehat{\mathbf{y}}_i). \tag{A1}$$

For the representation extractor  $F_{sc}$ :

$$\mathcal{L}_{SC} = -\log \frac{\exp(\mathbf{h}^{\top} \mathbf{h}^{+} / \tau)}{\exp(\mathbf{h}^{\top} \mathbf{h}^{+} / \tau) + \sum_{K}^{k=1} \exp(\mathbf{h}^{\top} \mathbf{h}_{k}^{-} / \tau)}$$
(A2)

where  $\mathbf{h}^+$ ,  $\mathbf{h}^-$ , K and  $\tau > 0$  are the positive example (have the same class label with  $\mathbf{h}$ ), negative example (have a different class label to  $\mathbf{h}$ ), the number of  $\mathbf{h}^-$  in the batch, a temperature parameter, respectively.

DRG training:

$$\mathcal{L}'_{adv} = W'_{adv} - \lambda'_{gpadv} \mathcal{L}'_{gpadv}, \qquad (A3)$$

$$W'_{adv} = \mathbb{E}[D'_{adv}(\mathbf{r}_0, \mathbf{a})] - \mathbb{E}[D'_{adv}(\tilde{\mathbf{r}}_0, \mathbf{a})], \quad (A4)$$

$$\mathcal{L}'_{apady} = \mathbb{E}[(\|\nabla_{\hat{\mathbf{r}}_0} D'_{ady}(\hat{\mathbf{r}}_0, \mathbf{a})\|_2 - 1)^2], \quad (A5)$$

$$\mathcal{L}'_{diff} = W'_{diff} - \lambda'_{qpdiff} \mathcal{L}'_{qpdiff}, \quad (A6)$$

$$W'_{diff} = \mathbb{E}[D'_{diff}(\mathbf{r}_{t-1}, \mathbf{r}_t, \mathbf{a}, t)] - \mathbb{E}[D'_{diff}(\tilde{\mathbf{r}}_{t-1}, \mathbf{r}_t, \mathbf{a}, t)], \quad (A7)$$

$$\mathcal{L}'_{gpdiff} = \mathbb{E}[(\|\nabla_{\hat{\mathbf{r}}_{t-1}} D_{diff}(\hat{\mathbf{r}}_{t-1}, \mathbf{r}_t, \mathbf{a}, t)\|_2 - 1)^2], \tag{A8}$$

#### Algorithm 1 Fine-Tuning of ZeroDiff

**Input**: Training data  $\mathcal{D}^{tr} = \{(x^s, a^s, y^s) | x^s \in \mathcal{X}^s, a^s \in \mathcal{A}^s, y^s \in \mathcal{Y}^s\}$ , the iteration number for fine-tuning  $N_{ft}$ .

#### [Fine-tuning with CE and SC]

Define  $F_{ce}$  and  $F_{cls}$  as pretrained feature extractor and feature classifier.

Define  $F_{sc}$  and  $F_{pro}$  as pretrained representation extractor and contrastive projector.

## for $N_{ft}$ do.

Draw a batch of samples  $(x^s, a^s, y^s)$  from  $\mathcal{D}^{tr}$ . Extract feature  $v^s \leftarrow F_{ce}(x^s)$ .

Classify feature  $\hat{y}^s \leftarrow F_{cls}(v^s)$ .

Update  $F_{ce}$  and  $F_{cls}$  with  $\mathcal{L}_{CE}$  by Eq. A1. Extract representation  $r^s \leftarrow F_{sc}(x^s)$ .

Project representation into contrastive space  $h^s \leftarrow F_{pro}(r^s)$ .

Update  $F_{sc}$  and  $H_{sc}$  with  $\mathcal{L}_{SC}$  by Eq. A2.

#### end for

Freeze  $F_{ce}$  and  $F_{sc}$  as  $F_{ce}^*$  and  $F_{sc}^*$ .

Output:  $F_{ce}^*$  and  $F_{sc}^*$ .

#### Algorithm 2 Generator Training of ZeroDiff

**Input**: Training data  $\mathcal{D}^{tr} = \{(x^s, a^s, y^s) | x^s \in \mathcal{X}^s, a^s \in \mathcal{A}^s, y^s \in \mathcal{Y}^s\}$ , the iteration number for generator training  $N_g$ , the iteration number for discriminator in a step  $N_{dis}$ .

## [Training DRG]

Define R as diffusion-based representation generator.

Define  $D'_{adv}$  and  $D'_{diff}$  as clean representation discriminator and noised representation discriminator.

#### for $N_g$ do

Draw a batch of samples  $(x^s, a^s, y^s)$  from  $\mathcal{D}^{tr}$ . for  $N_{dis}$  do

Extract clean contrastive representation  $r_0^s \leftarrow F_{sc}^*(x^s)$ .

Sample  $t \sim U(0, T-1)$ .

Add noise into clean representation at t and t+1 as  $r_t^s$  and  $r_{t+1}^s$  by Eq. 1.

Generate fake clean representation  $\tilde{r}_0^s \leftarrow R(z, a^s, r_{t+1}^s, t), z \sim \mathcal{N}(0, I).$ 

Renoise fake representation  $\tilde{r}_t^s$  by Eq. 6. Update  $D'_{adv}$  and  $D'_{diff}$  by minimizing Eq. A3 and Eq. A6.

#### end for

Update R by maximizing  $\mathcal{L}'_{adv}$  and  $\mathcal{L}'_{diff}$ . end for

Freeze R as  $R^*$ .

#### [Training DFG]

Define G as diffusion-based feature generator. Define  $D_{adv}$ ,  $D_{diff}$  and  $D_{rep}$  as discriminators for clean feature, noised feature and contrastive representation aspects.

## for $N_g$ do

Draw a batch of samples  $(x^s, a^s, y^s)$  from  $\mathcal{D}^{tr}$ . for  $N_{dis}$  do

Extract clean representation  $r_0^s \leftarrow F_{sc}^*(x^s)$  and feature  $v_0^s \leftarrow F_{ce}^*(x^s)$ .

Sample  $t \sim U(0, \cdots, T-1)$ .

Noising feature at t and t+1 as  $v_t^s$  and  $v_{t+1}^s$  by Eq. 1.

Generate fake clean feature  $\tilde{v}_0^s \leftarrow G(z, a^s, r_0^s, v_{t+1}^s, t), z \sim \mathcal{N}(0, I).$ 

Renoise fake feature  $\tilde{v}_t^s$  by Eq. 6.

 $\mbox{Update $D_{adv}$, $D_{diff}$ and $D_{rep}$ by minimizing Eq. 3, Eq. 9, Eq. 13 and Eq. 16. }$ 

#### end for

Update G by maximizing Eq. 3, Eq. 9 and Eq. 13. .

#### end for

Freeze G as  $G^*$ .

Output:  $G^*$  and  $R^*$ .

Table A1: The hyper-parameter settings of our ZeroDiff and baselines. We evaluate generation methods with their official recommended hyper-parameters, including the synthesizing number of per unseen classes  $N_{syn}$ , the learning rate  $\lambda_{lr}$ , batch size  $N_b$ . For limited training set, we only change the  $N_{syn}$  according to sample remaining ratio.

Method		AWA2			CUB		SUN			
Wicoliod	$N_{syn}$	$\lambda_{lr}$	$N_b$	$N_{syn}$	$\lambda_{lr}$	$N_b$	$\overline{N_{syn}}$	$\lambda_{lr}$	$N_b$	
f-VAEGAN	1800	0.00001	64	300	0.0001	64	400	0.0001	64	
SDVAE	5400	0.00003	64	1200	0.0001	64	1200	0.0003	64	
CEGAN	1800	0.0001	4096	300	0.0001	2048	100	0.00005	1024	
DFCAFlow	60000	0.0003	256	600	0.0003	256	120	0.0003	256	
ZeroDiff	12000	0.0005	64	1440	0.0002	64	400	0.0001	64	

### Algorithm 3 ZSL Testing of ZeroDiff

**Input**: Testing dataset  $\mathcal{D}^{te} = \{(x^u, a^u, y^u) | x^u \in$  $\mathcal{X}^u, a^u \in \mathcal{A}^u, y^u \in \mathcal{Y}^u$ , trained DFG  $F^*$  and DRG  $R^*$ , the iteration number for pseudo training  $N_{te}$ , the generation number per class  $N_{syn}$ .

#### [Testing DFG and DRG]

for every unseen class  $c^u$  do

Define  $\tilde{y}^u$  as copying  $c^u$   $N_{syn}$  times and  $\tilde{a}^u$ as class semantics.

Generate fake clean representation  $\tilde{r}_0^s \leftarrow$  $R^*(z, a^u, r_T^u, T - 1), z, r_T^u \sim \mathcal{N}(0, I).$ 

Generate fake clean feature  $\tilde{v}_0^s$  $G^*(z, a^u, \tilde{r}_0^s, v_T^u, T-1), z, v_T^u \sim \mathcal{N}(0, I).$ 

Construct a new dataset  $\tilde{\mathcal{D}}^{te} = \{(\tilde{v}_0^s, \tilde{r}_0^s, \tilde{a}^u, \tilde{y}^u)\}.$ Define  $F_{zsl}$  as the final ZSL classifier.

Draw a batch of samples  $(\tilde{v}_0^u, \tilde{r}_0^u, \tilde{a}^u, \tilde{y}^u)$  from  $\tilde{\mathcal{D}}^{te}$ .

Classify pseudo sample  $\hat{y}^u \leftarrow F_{zsl}(\tilde{v}_0^u, \tilde{r}_0^u)$ . Update  $F_{zsl}$  with  $\mathcal{L}_{CE}$  by Eq. A1.

#### end for

Freeze  $F_{zsl}$  as  $F_{zsl}^*$ . **for** every real  $x^u$  **do** 

Extract clean contrastive representation  $r_0^u \leftarrow$  $F_{sc}^*(x^u)$  and clean feature  $v_0^u \leftarrow F_{ce}^*(v^u)$ .

Classify real sample  $\hat{y}^u \leftarrow F_{zsl}^*(v_0^u, r_0^u)$ . end for

Output: ZSL classification results  $\{(\hat{y}^u)\}$ .

#### Hyper-parameters

We also provide the hyper-parameter details of our reproduced methods in the Table A1.

## References

Akata Z, Reed S, Walter D, et al (2015) Evaluation of output embeddings for fine-grained image classification. In: Proceedings of the IEEE conference on computer vision and pattern recognition, pp 2927-2936

Arjovsky M, Chintala S, Bottou L (2017) Wasserstein generative adversarial networks. In: Precup D, Teh YW (eds) Proceedings of the 34th International Conference on Machine Learning, Proceedings of Machine Learning Research, vol 70. PMLR, pp 214–223

Badirli S, Akata Z, Mohler G, et al (2021) Finegrained zero-shot learning with dna as side information. Advances in Neural Information Processing Systems 34:19352–19362

Chao WL, Changpinyo S, Gong B, et al (2016) An empirical study and analysis of generalized zeroshot learning for object recognition in the wild. In: European conference on computer vision, Springer, pp 52–68

Chen S, Xie G, Liu Y, et al (2021a) Hsva: Hierarchical semantic-visual adaptation for zeroshot learning. Advances in Neural Information Processing Systems 34

Chen S, Hong Z, Hou W, et al (2022a) Transzero++: Cross attribute-guided transformer for zero-shot learning. IEEE transactions on pattern analysis and machine intelligence

Chen S, Hong Z, Liu Y, et al (2022b) Transzero: Attribute-guided transformer for zero-shot

- learning. In: AAAI
- Chen S, Hong Z, Xie GS, et al (2022c) Msdn: Mutually semantic distillation network for zeroshot learning. In: Proceedings of the IEEE/CVF conference on computer vision and pattern recognition, pp 7612–7621
- Chen YH, Yeh MC (2021) Text-enhanced attributebased attention for generalized zero-shot finegrained image classification. In: Proceedings of the 2021 International Conference on Multimedia Retrieval, pp 447–450
- Chen Z, Luo Y, Qiu R, et al (2021b) Semantics disentangling for generalized zero-shot learning. In: Proceedings of the IEEE/CVF international conference on computer vision, pp 8712–8720
- Clark K, Jaini P (2024) Text-to-image diffusion models are zero shot classifiers. Advances in Neural Information Processing Systems 36
- Cui J, Zhong Z, Liu S, et al (2021) Parametric contrastive learning. In: Proceedings of the IEEE/CVF international conference on computer vision, pp 715–724
- Cui J, Zhong Z, Tian Z, et al (2023) Generalized parametric contrastive learning. IEEE Transactions on Pattern Analysis and Machine Intelligence
- Deng J, Dong W, Socher R, et al (2009) Imagenet: A large-scale hierarchical image database. In: 2009 IEEE conference on computer vision and pattern recognition, Ieee, pp 248–255
- Ding Z, Shao M, Fu Y (2017) Low-rank embedded ensemble semantic dictionary for zero-shot learning. In: Proceedings of the IEEE conference on computer vision and pattern recognition, pp 2050–2058
- Gao R, Wan F, Organisciak D, et al (2022) Absolute zero-shot learning. arXiv preprint arXiv:220211319
- Gulrajani I, Ahmed F, Arjovsky M, et al (2017) Improved training of wasserstein gans. Advances in neural information processing systems 30

- Han Z, Fu Z, Chen S, et al (2021) Contrastive embedding for generalized zero-shot learning. In: Proceedings of the IEEE/CVF Conference on Computer Vision and Pattern Recognition, pp 2371–2381
- He K, Zhang X, Ren S, et al (2016) Deep residual learning for image recognition. In: Proceedings of the IEEE conference on computer vision and pattern recognition, pp 770–778
- Ho J, Jain A, Abbeel P (2020) Denoising diffusion probabilistic models. Advances in Neural Information Processing Systems 33:6840–6851
- Islam A, Chen CFR, Panda R, et al (2021) A broad study on the transferability of visual representations with contrastive learning. In: Proceedings of the IEEE/CVF International Conference on Computer Vision, pp 8845–8855
- Jiang C, Shen Y, Chen D, et al (2024) Estimation of near-instance-level attribute bottleneck for zeroshot learning. International Journal of Computer Vision pp 1–27
- Jiang Z, Chen T, Chen T, et al (2021) Improving contrastive learning on imbalanced data via open-world sampling. Advances in Neural Information Processing Systems 34:5997–6009
- Li AC, Prabhudesai M, Duggal S, et al (2023) Your diffusion model is secretly a zero-shot classifier.
   In: Proceedings of the IEEE/CVF International Conference on Computer Vision, pp 2206–2217
- Li T, Katabi D, He K (2024) Return of unconditional generation: A self-supervised representation generation method. 2312.03701
- Li X, Xu Z, Wei K, et al (2021) Generalized zeroshot learning via disentangled representation.
   In: Proceedings of the AAAI Conference on Artificial Intelligence, pp 1966–1974
- Liu M, Li F, Zhang C, et al (2023) Progressive semantic-visual mutual adaption for generalized zero-shot learning. In: Proceedings of the IEEE/CVF Conference on Computer Vision and Pattern Recognition, pp 15337–15346

- Naeem MF, Xian Y, Gool LV, et al (2022) I2dformer: Learning image to document attention for zero-shot image classification. Advances in Neural Information Processing Systems 35:12283–12294
- Narayan S, Gupta A, Khan FS, et al (2020) Latent embedding feedback and discriminative features for zero-shot classification. In: Computer Vision–ECCV 2020: 16th European Conference, Glasgow, UK, August 23–28, 2020, Proceedings, Part XXII 16, Springer, pp 479–495
- Nowozin S, Cseke B, Tomioka R (2016) f-gan: Training generative neural samplers using variational divergence minimization. Advances in neural information processing systems 29
- Patterson G, Hays J (2012) Sun attribute database: Discovering, annotating, and recognizing scene attributes. In: 2012 IEEE Conference on Computer Vision and Pattern Recognition, IEEE, pp 2751–2758
- Reed S, Akata Z, Lee H, et al (2016) Learning deep representations of fine-grained visual descriptions. In: Proceedings of the IEEE conference on computer vision and pattern recognition, pp 49–58
- Rombach R, Blattmann A, Lorenz D, et al (2022) High-resolution image synthesis with latent diffusion models. In: Proceedings of the IEEE/CVF conference on computer vision and pattern recognition, pp 10684–10695
- Sohl-Dickstein J, Weiss E, Maheswaranathan N, et al (2015) Deep unsupervised learning using nonequilibrium thermodynamics. In: International conference on machine learning, PMLR, pp 2256–2265
- Song J, Meng C, Ermon S (2020a) Denoising diffusion implicit models. In: International Conference on Learning Representations
- Song Y, Sohl-Dickstein J, Kingma DP, et al (2020b) Score-based generative modeling through stochastic differential equations. arXiv preprint arXiv:201113456

- Su H, Li J, Lu K, et al (2023) Dual-aligned feature confusion alleviation for generalized zero-shot learning. IEEE Transactions on Circuits and Systems for Video Technology
- Tang B, Zhang J, Yan L, et al (2024) Data-free generalized zero-shot learning. In: Proceedings of the AAAI Conference on Artificial Intelligence, pp 5108–5117
- Verma VK, Arora G, Mishra A, et al (2018) Generalized zero-shot learning via synthesized examples. In: Proceedings of the IEEE conference on computer vision and pattern recognition, pp 4281–4289
- Verma VK, Brahma D, Rai P (2020) Metalearning for generalized zero-shot learning. In: Proceedings of the AAAI conference on artificial intelligence, pp 6062–6069
- Wang Z, Hao Y, Mu T, et al (2023) Bi-directional distribution alignment for transductive zero-shot learning. In: Proceedings of the IEEE/CVF Conference on Computer Vision and Pattern Recognition, pp 19893–19902
- Welinder P, Branson S, Mita T, et al (2010) Caltech-ucsd birds 200
- Xian Y, Lampert CH, Schiele B, et al (2018a) Zeroshot learning—a comprehensive evaluation of the good, the bad and the ugly. IEEE transactions on pattern analysis and machine intelligence 41(9):2251–2265
- Xian Y, Lorenz T, Schiele B, et al (2018b) Feature generating networks for zero-shot learning. In: Proceedings of the IEEE conference on computer vision and pattern recognition, pp 5542–5551
- Xian Y, Sharma S, Schiele B, et al (2019) f-vaegand2: A feature generating framework for any-shot learning. In: Proceedings of the IEEE/CVF conference on computer vision and pattern recognition, pp 10275–10284
- Xiao Z, Kreis K, Vahdat A (2022) Tackling the generative learning trilemma with denoising diffusion GANs. In: International Conference on Learning Representations

- Xu W, Xian Y, Wang J, et al (2020) Attribute prototype network for zero-shot learning. In: NeurIPS
- Xu W, Xian Y, Wang J, et al (2022) Attribute prototype network for any-shot learning. International Journal of Computer Vision 130(7):1735— 1753
- Yang FE, Lee YH, Lin CC, et al (2023) Semantics-guided intra-category knowledge transfer for generalized zero-shot learning. International Journal of Computer Vision 131(6):1331–1345
- Yang Y, Luo Y, Chen W, et al (2016) Zero-shot hashing via transferring supervised knowledge.
  In: Proceedings of the 24th ACM international conference on Multimedia, pp 1286–1295
- Ye Z, Hu F, Lyu F, et al (2021) Disentangling semantic-to-visual confusion for zero-shot learning. IEEE Transactions on Multimedia
- Ye Z, Yang G, Jin X, et al (2023) Rebalanced zero-shot learning. IEEE Transactions on Image Processing
- Zhang Y, Xiang T, Hospedales TM, et al (2018) Deep mutual learning. In: Proceedings of the IEEE conference on computer vision and pattern recognition, pp 4320–4328
- Zhao S, Ren H, Yuan A, et al (2018) Bias and generalization in deep generative models: An empirical study. Advances in Neural Information Processing Systems 31
- Zhu J, Wang Z, Chen J, et al (2022) Balanced contrastive learning for long-tailed visual recognition. In: Proceedings of the IEEE/CVF Conference on Computer Vision and Pattern Recognition, pp 6908–6917
- Zhu Y, Elhoseiny M, Liu B, et al (2018) A generative adversarial approach for zero-shot learning from noisy texts. In: Proceedings of the IEEE conference on computer vision and pattern recognition, pp 1004–1013